Microelectronic Engineering 88 (2011) 605–609

Contents lists available at ScienceDirect

Microelectronic Engineering

journal homepage: www.elsevier.com/locate/mee

Crystalline orientation dependence of electrical properties of Mn Germanide/Ge(1 1 1) and (0 0 1) Schottky contacts

Tsuyoshi Nishimura, Osamu Nakatsuka *, Shingo Akimoto, Wakana Takeuchi, Shigeaki Zaima

Department of Crystalline Materials Science, Graduate School of Engineering, Nagoya University, Furo-cho, Chikusa-ku, Nagoya 464-8603, Japan

ARTICLE INFO

Article history:
Available online 20 August 2010

Keywords:
Manganese
Germanium
Epitaxial growth
Schottky barrier height
Fermi level pinning
Contact

ABSTRACT

We have investigated the crystalline orientation dependence of the electrical properties of Mn germanide/Ge(1 1 1) and (0 0 1) Schottky contacts. We prepared epitaxial and polycrystalline Mn_5Ge_3 layers on Ge(1 1 1) and (0 0 1) substrates, respectively. The Schottky barrier height (SBH) estimated from the current density-voltage characteristics for epitaxial Mn_5Ge_3/Ge(1 1 1) is as low as 0.30 eV, while the SBH of polycrystalline Mn_5Ge_3/Ge(0 0 1) is higher than 0.56 eV. On the other hand, the SBH estimated from capacitance–voltage characteristics are higher than 0.6 eV for both samples. The difference of these SBHs can be explained by the local carrier conduction through the small area with the low SBH regions in the epitaxial Mn_5Ge_3/Ge(1 1 1) contact. This result suggests the possibility that the lowering SBH takes place due to Fermi level depinning in epitaxial germanide/Ge(1 1 1) contacts.

1. Introduction

Ge is one of the most attractive channel materials for next generation metal-oxide-semiconductor field effect transistors (MOSFETs) because both electron and hole mobility of Ge are higher than Si [1]. For realizing high performance Ge channel MOSFETs, lowering the parasitic resistance at source/drain (S/D) and metal/Ge contact regions is required. The control of Schottky barrier height (SBH) at a metal/Ge interface is one of the key issues in order to achieve a low contact resistance, because the contact resistivity of the metal/semiconductor interface exponentially decreases with decreasing in SBH. The SBH essentially depends on the work function of a metal in the Schottky limit condition. However, in practice, it is known that SBHs of various metal/Ge contacts hardly depend on the metal work function, because the Fermi level pinning (FLP) occurs at metal/Ge contacts [2,3]. SBHs of metal/*n*-type Ge contacts generally exhibit higher values than 0.5 eV. Although some reports discussed the origin of FLP as metal induced gap states (MIGS) or disorder induced gap states (DIGS), the detail of FLP in metal/Ge contacts has not been clarified yet.

On the other hand, some technologies for SBH modulation of metal/Ge contacts have been proposed from other reports; the introduction of an ultra thin insulator interfacial layer [4,5] and the segregation of sulfur at the NiGe/Ge interface [6]. However, the detailed mechanism of SBH modulation has not been understood well. Therefore, understanding the origin of FLP and the establishing the technology of SBH modulation are very important issues.

In this study, we took note of the interface crystalline structure of the metal/Ge contacts. In general, a contact layer such as metal germanide consists of polycrystalline grains, and there are a lot of defects such as dangling bonds at the interface between a polycrystalline germanide layer and a Ge substrate. These defects at the interface certainly contribute to FLP. We expect to reduce such dangling bonds by using an epitaxial metal/Ge contact, because the atomic bonding structure can be modulated from random of the polycrystalline interface to lattice-matched. Gaudet et al. investigated reaction of transition metal with Ge substrates and formation of various germanides [7]. Schottky diode properties of metal/Ge contacts have been also reported [8,9]. However, there are few studies about the relationship between the electrical properties and the interface crystalline structure. Here, we focused on manganese germanide, Mn_5Ge_3 for contact material, because it is well known that Mn_5Ge_3 can be epitaxially grown on a Ge(1 1 1) substrate [10]. In particular, we can prepare an epitaxial Mn_5Ge_3 layer by using the deposition of a Mn thin layer and post-deposition annealing (PDA). Germanidation using solid-phase reaction is more familiar for the integrated circuit process compared to molecular beam epitaxy (MBE) or solid-phase epitaxy (SPE) method. In this study, we demonstrate that we are able to prepare two types of the interface crystalline structure of Mn germanide layers on Ge substrates by changing the crystalline structure of substrates, *i.e.* polycrystalline Mn_5Ge_3/Ge(0 0 1) and epitaxial Mn_5Ge_3/Ge(1 1 1) contacts. We also investigated the difference of

* Corresponding author. Tel.: +81 52 789 3819; fax: +81 52 789 2760.
E-mail address: nakatuka@alice.xtal.nagoya-u.ac.jp (O. Nakatsuka).

0167-9317/$ - see front matter © 2010 Elsevier B.V. All rights reserved.
doi:10.1016/j.mee.2010.08.014

crystalline and electrical properties of both Mn_5Ge_3/Ge contacts and discuss the SBHs behavior of these contacts.

2. Experiments

Substrates used were *n*-type Ge(0 0 1) and Ge(1 1 1) wafers with the resistivities of 2.3–4.9 and 0.1–1 Ω cm, respectively. We also used *p*-type Ge(1 1 1) wafers. After SiO_2 layer was deposited on wafers by spin-coating method, contact holes whose area size of $1 \times 1\ mm^2$ were patterned with photolithography technique for preparing Schottky diodes. A Ge substrate was dipped into a diluted HF solution and deionized water, alternately. Then, the sample was loaded into an ultra high vacuum (UHV) chamber whose base pressure was below 2×10^{-7} Pa and was annealed at 550 °C for 30 min to remove native oxide on the Ge surface. A 20-nm-thick Mn layer was successively deposited in the UHV chamber by using e-gun evaporation. Then, the sample was annealed at a temperature ranging from 350 to 550 °C for 15 min in the same chamber. After annealing of the sample, Al electrodes were deposited in a conventional chamber by resistance heating for preparing the Schottky diodes.

X-ray diffraction (XRD) and transmission electron microscopy (TEM) were carried out to investigate the crystalline structure and the morphology of Mn germanide layers. Electrical properties were measured by current density–voltage (*J*–*V*) characteristics, capacitance–voltage (*C*–*V*) characteristics, and deep level optical transient spectroscopy (DLTS).

3. Results and discussion

Fig. 1(a and b) shows XRD (2θ-scan) and (2θ/ω-scan) profiles, respectively, of Mn/Ge(0 0 1) and Ge(1 1 1) samples after annealing at 350 and 500 °C. In the 2θ-scan measurement of Mn/Ge(0 0 1) samples, diffraction peaks corresponding to polycrystalline Mn_5Ge_3 can be clearly observed after annealing at each temperature as shown in Fig. 1(a). On the other hand, in the case of Mn/Ge(1 1 1) samples, no peaks are observed after annealing in 2θ-scan profiles. We can observe diffraction peaks corresponding to Mn_5Ge_3 0 0 2 and 0 0 4 in the 2θ/ω-scan profiles of Mn/Ge(1 1 1) samples as shown in Fig. 1(b). These results strongly indicate that an epitaxial, not polycrystalline Mn_5Ge_3 layer is dominantly formed in these Ge(1 1 1) samples.

Fig. 2(a and b) shows cross-sectional TEM images of Mn/Ge(0 0 1) and Ge(1 1 1) samples, respectively, after annealing at 350 °C. Fig. 2(c) also shows the typical transmission electron diffraction (TED) pattern of the Mn germanide layer grown on a Ge(1 1 1) substrate at 420 °C. TEM and XRD observation for all samples revealed that polycrystalline and epitaxial Mn_5Ge_3 layers were formed on Ge(0 0 1) and Ge(1 1 1) substrates, respectively, after annealing at a temperature ranging from 350 to 500 °C. The TED pattern indicates the epitaxial growth of Mn_5Ge_3 on a Ge(1 1 1) substrate with the crystalline relationship of Mn_5Ge_3(0 0 1)//Ge(1 1 1) and Mn_5Ge_3[100]//Ge[1 $\bar{1}$ 0]. The interface between an epitaxial Mn_5Ge_3 layer and a Ge(1 1 1) substrate is smooth. In contrast, the interface between polycrystalline Mn_5Ge_3 and Ge(0 0 1) is rough due to undulation of grain boundaries of Mn germanide crystallites.

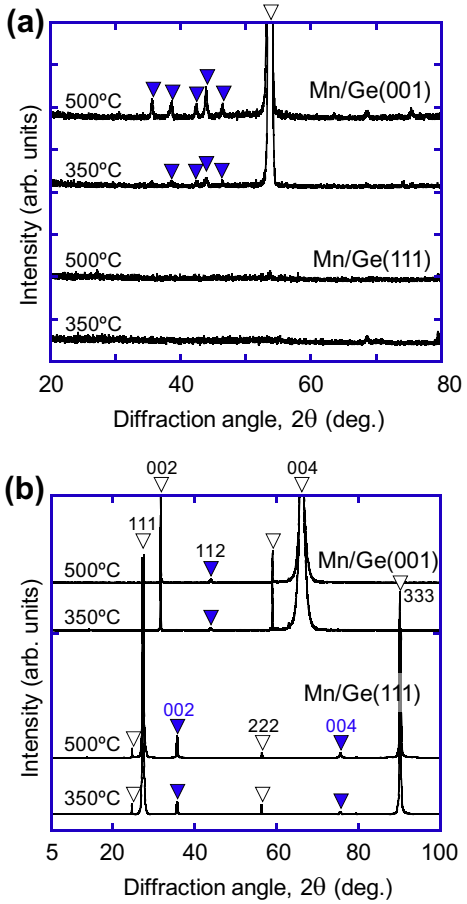

Fig. 1. XRD (a) 2θ-scan and (b) 2θ/ω-scan profiles for Mn/Ge(0 0 1) and Ge(1 1 1) samples after annealing from 350 to 500 °C. Solid and open triangles indicate the diffraction peak positions related to Mn_5Ge_3 and Ge, respectively.

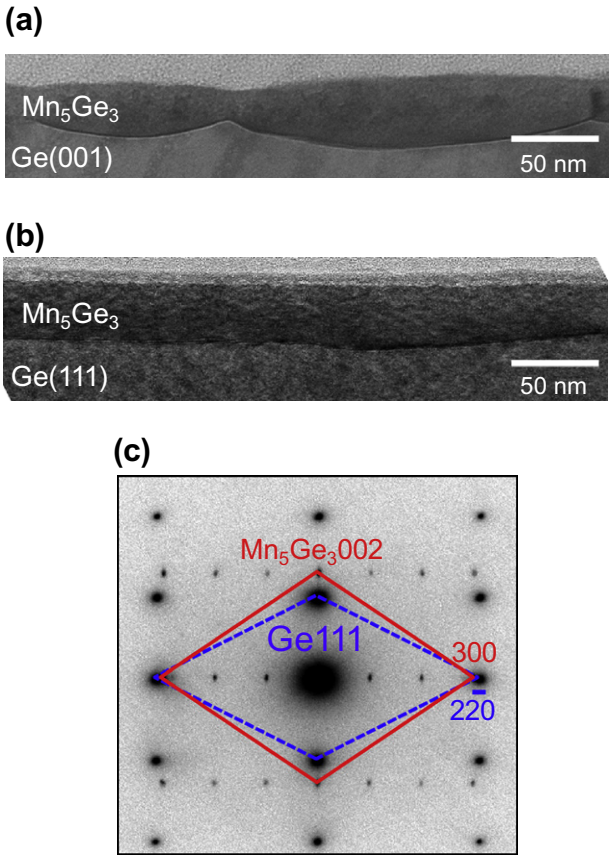

Fig. 2. Cross-sectional TEM images of (a) Mn/Ge(0 0 1) and (b) Mn/Ge(1 1 1) samples annealed at 350 °C, (c) TED pattern of the Mn germanide/Ge(1 1 1) sample annealed at 420 °C. The red solid and blue broken lines indicate reciprocal lattice cells of Mn_5Ge_3 and Ge, respectively.

Fig. 3(a and b) shows the forward current density–voltage (J–V) characteristics of the epitaxial Mn_5Ge_3/n-type Ge(1 1 1) and Ge(0 0 1) Schottky diodes, respectively, for various temperatures ranging from 100 to 300 K. These samples were annealed at 350 °C. The J–V characteristic of thermionic emission current is theoretically expressed;

$$J = J_s \exp\left(\frac{q(V - IR_s)}{nk_BT} - 1\right), \tag{1}$$

and the saturation current density J_s is

$$J_s = A^*T^2 \exp\left(-\frac{q\phi_{Bn}}{k_BT}\right), \tag{2}$$

where q is the elementary charge, n is the ideality factor, k_B is the Boltzmann constant, T is the temperature, I is the current, R_s is the substrate resistance, A^* is the effective Richardson constant, ϕ_{Bn} is the SBH [11]. Fig. 3(c and d) shows Arrhenius plots of the saturation current density and the ideality factors estimated from J–V characteristics of the both samples. The ideality factors at above 200 K are as low as unity, meaning that the thermionic emission current is the dominant conduction mechanism. The SBH of the Mn_5Ge_3/Ge(1 1 1) sample at this temperature range is estimated to be 0.30 ± 0.01 eV from the slope of the Arrhenius plot of the saturation current density by using the theory of thermionic emission current conduction as shown in Eqs. (1) and (2).

J–V curves measured near the room temperature also exhibit good thermionic emission current characteristics for other Mn_5Ge_3/n-type Ge(0 0 1) and Ge(1 1 1) samples. The SBH for the polycrystalline Mn_5Ge_3/n-type Ge(0 0 1) sample annealed at 500 °C was estimated to be 0.56 eV from the J–V characteristics. We also prepared an epitaxial Mn_5Ge_3 layer on p-type Ge(1 1 1) sample and evaluated the SBH of this contact. However the J–V characteristics of the Mn_5Ge_3/p-Ge(1 1 1) contact exhibits the Ohmic properties and the SBH could not be estimated.

We also measured capacitance–voltage (C–V) characteristics of the Mn germanide/Ge Schottky diodes at 100 K. The C–V characteristic of Schottky contact is theoretically expressed;

$$\frac{1}{C^2} = \frac{2(qV_{bi} - qV - k_BT)}{q^2\varepsilon_s N_D} \tag{3}$$

and the SBH ϕ_{Bn} is

$$\phi_{Bn} = V_{bi} + V_n \tag{4}$$

$$V_n = k_BT \ln\left(\frac{N_C}{N_D}\right) \tag{5}$$

where ε_s is the permittivity, N_D is the density of impurity, V_{bi} is the built-in potential, N_C is the effective density of state [11]. The SBHs were estimated by using Eqs. (3)–(5) to be about same values of 0.6–0.7 eV for both epitaxial Mn_5Ge_3/Ge(1 1 1) and polycrystalline Mn_5Ge_3/Ge(0 0 1) samples.

The SBHs estimated from the J–V and C–V characteristics for various samples are summarized in Table 1. The SBH values of polycrystalline Mn_5Ge_3/Ge(0 0 1) samples are higher than 0.5 eV for both J–V and C–V characteristics. On the other hand, for epitax-

Table 1
Summary of Schottky barrier heights estimated from J–V and C–V characteristics for Mn germanide/Ge contacts.

Contact structure	Annealing temperature (°C)	Schottky barrier height (eV)	
		J–V (at RT)	C–V (at 100 K)
Polycrystalline Mn_5Ge_3/	350	0.56 ± 0.05	0.63 ± 0.01
n-Ge(0 0 1)	500	0.56 ± 0.01	0.68 ± 0.01
Epitaxial Mn_5Ge_3/n-Ge(1 1 1)	350	0.30 ± 0.01	0.67 ± 0.02
	500	0.43	0.72 ± 0.01
Epitaxial Mn_5Ge_3/p-Ge(1 1 1)	350	Ohmic	NA

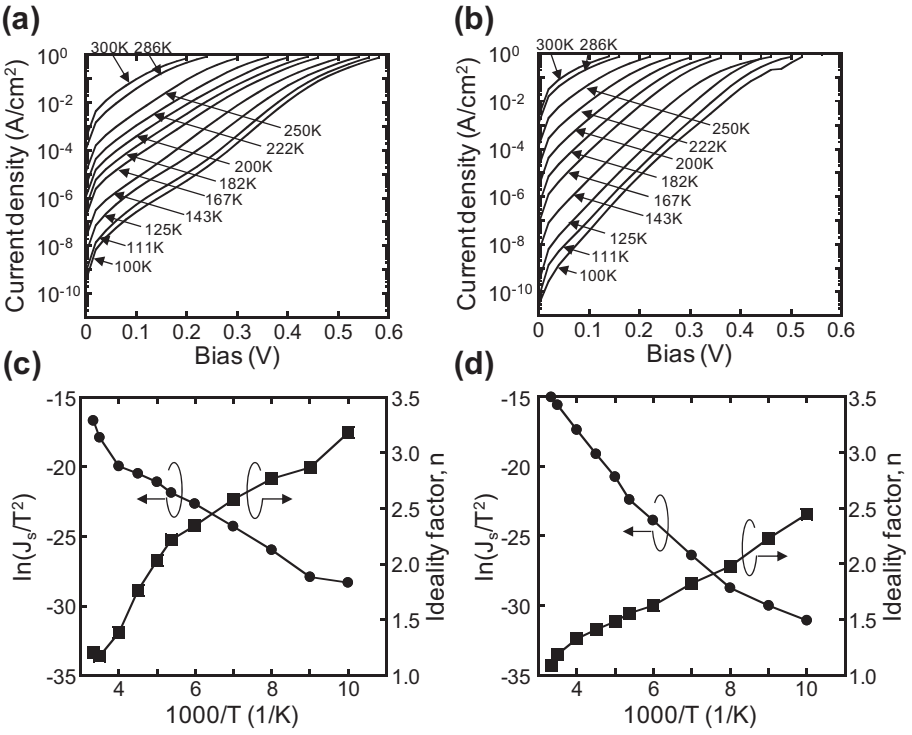

Fig. 3. Forward current voltage characteristics of (a) the Mn_5Ge_3/n-Ge(0 0 1) and (b) the Mn_5Ge_3/n-Ge(1 1 1) Schottky diode annealed at 350 °C for various temperature. Arrhenius plots of $\ln(J_s/T^2)$ and the ideality factor for (c) the Mn_5Ge_3/n-Ge(0 0 1) and (d) the Mn_5Ge_3/n-Ge(1 1 1) contacts, respectively.

ial Mn_5Ge_3/Ge(1 1 1) samples, the values estimated from *J–V* characteristics are as low as between 0.30 and 0.43 eV. However, in the case of *C–V* characteristics, the estimated SBHs of epitaxial Mn_5Ge_3/Ge(1 1 1) samples are high, comparable to polycrystalline Mn_5Ge_3/Ge(0 0 1) samples.

Here, we deduce the reason of the different SBHs between the *J–V* and *C–V* characteristics for the epitaxial Mn germanide/Ge(1 1 1) contact. We consider that there are two different regions with low and high SBHs at the interface between epitaxial a Mn_5Ge_3 layer and a Ge substrate. For *J–V* characteristics, the current density depends exponentially on SBH as shown in Eq. (2). Therefore, the low SBH region dominates the current conduction, even if the area of the region is rather smaller than that of the high SBH region. On the other hand, for *C–V* characteristics, the capacitance of the high SBH region, whose area is larger than the low SBH, dominates *C–V* characteristics. Tung previously reported the crystalline orientation dependence of SBH on epitaxial $CoSi_2$ and $NiSi_2$ films on Si substrates [12,13]. They reported in homogeneity of the SBH for epitaxial $NiSi_2$/*p*-Si(0 0 1) diodes and discrepancies between SBHs measured by *I–V* and *C–V* techniques. Our results for Mn_5Ge_3/Ge are similar to them. These results suggest that there is the possibility that the FLP is locally resolved in the epitaxial Mn_5Ge_3/Ge(1 1 1) samples and the local carrier conduction through such low SBH regions takes place, by contrast, the FLP strongly occurs in polycrystalline Mn_5Ge_3/Ge(0 0 1) samples.

Many researchers previously reported that the theoretical model for the interface consisting of two different SBHs [14–16]. Fig. 4 shows the calculation result of the apparent SBH as a function of the fraction of area of the low SBH region occupied total contact area, according to their model. In this calculation, we assume that two different SBHs exist in the epitaxial Mn_5Ge_3/Ge(1 1 1) interface; high SBH, ϕ_{BH} of 0.66 eV and the low SBH, ϕ_{BL} of 0.20, 0.25, and 0.30 eV is to be estimated by *J–V* characteristics. The apparent of SBH increases with the exponential reduction in the fraction of the area of low SBH region. Considering this model for Mn germanide/Ge(1 1 1) samples in this study, the fraction of the effective contact area of the low SBH against the total contact area is estimated to be less than 0.01.

We also estimated the Richardson constant of *J–V* characteristic in order to consider the dominant conduction area in the contact area. The Richardson constants of polycrystalline Mn_5Ge_3/*n*-Ge(0 0 1) samples were estimated to be 34–55 A/cm^2 K^2 from *J–V* characteristics by using Eq. (2). The Richardson constant for metal/semiconductor contacts is generally about 10–100 A/cm^2 K^2 [11], and the estimated values for polycrystalline Mn_5Ge_3 samples agree with it. On the other hand, the Richardson constants for epitaxial Mn_5Ge_3/Ge(1 1 1) samples were estimated to be very low

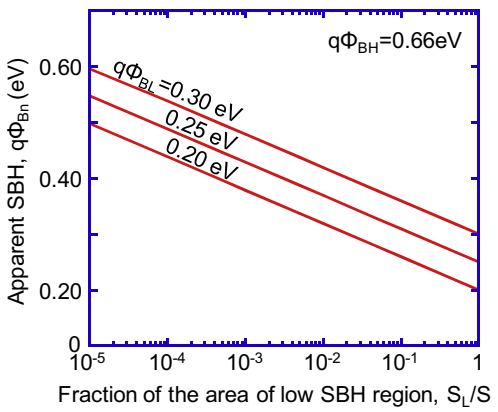

Fig. 4. The apparent SBH as a function of the fraction of area of the low SBH region occupied total contact area.

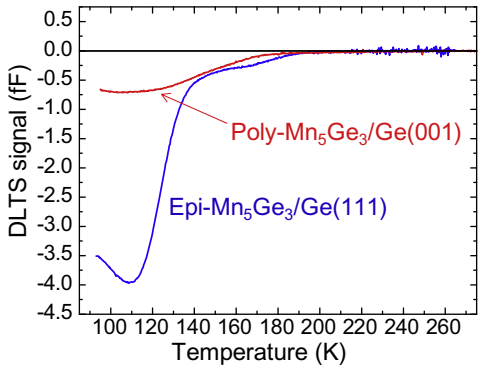

Fig. 5. DLTS spectra of polycrystalline and epitaxial Mn_5Ge_3/*n*-Ge samples annealed at 350 °C.

values of 0.06–0.17 A/cm^2 K^2. It is 2–3 orders of magnitude lower than that of the polycrystalline Mn germanide/Ge contacts. These results suggest that the practical area of the current conduction is quite small for the epitaxial Mn germanide/Ge contact, and the saturation current is underestimated owing to the overestimation of the contact area size (1 × 1 mm^2). According to above deduction about the Richardson constant, the fraction of the effective contact area of the low SBH region to total contact area is estimated to be less than 0.01 in epitaxial Mn_5Ge_3/Ge(1 1 1) contacts. This value basically agrees with that deduced in the consideration of the model of two different SBH areas as mentioned above.

Fig. 5 shows the DLTS spectra of polycrystalline and epitaxial Mn germanide/*n*-type Ge samples annealed at 350 °C. In the case of the polycrystalline Mn germanide/Ge(0 0 1) contact, a weak and broad signal is observed under 180 K. In the case of this sample, the activation energy of the defect state is estimated to be E_V + 0.13–0.17 eV. On the other hand, in the case of the Mn_5Ge_3/Ge(1 1 1) sample, a large and narrow signal is observed near 110 K, and the activation energy of the defect state can be estimated to E_V + 0.15 eV. These levels of defect center are probably related to Mn (E_V + 0.16 V), divacancy-donor (E_V + 0.10, 0.12 and 0.16 V), or complex of these defects [17]. Recently, Simoen et al. [18] examined the deep levels by DLTS for various metal/*n*-Ge samples. They reported that indiffusion of metal atoms occurs during the germanidation depending on the deposited metal and annealing temperature. In this study, this defect center is probably formed with germanidation. Note that the characteristics of defect states are obviously different between polycrystalline and epitaxial Mn germanide/*n*-Ge contacts. We suggest that these results exhibit the difference of the solid-phase reaction behavior and the interface structure which influences electrical properties for Schottky contacts. However, the detail of defect state has not been clarified yet.

4. Conclusions

We investigated the crystalline orientation dependence of electrical properties of Mn germanide/Ge(0 0 1) and (1 1 1) Schottky contacts. We demonstrated that we can prepare Mn_5Ge_3 layers on Ge substrates with the deferent crystalline structure, *i.e.* polycrystalline and epitaxial germanides by selecting the substrate crystalline orientations, (0 0 1) and (1 1 1), respectively. The SBH estimated from *J–V* characteristics of epitaxial Mn_5Ge_3/Ge(1 1 1) exhibits lower values than that of polycrystalline Mn_5Ge_3/Ge(0 0 1), although those of both samples from *C–V* characteristics is as high as 0.6 eV. We deduce that the Fermi level depinning takes place and SBH approaches to the Schottky limit at local regions in epitaxial Mn_5Ge_3/Ge(1 1 1) contacts. As a result, there is the local

carrier conduction through such regions of low SBH. Depinning of the Fermi level is probably caused by lowering of the density of interfacial defects, such as dangling bonds, at the epitaxial Mn_5Ge_3/Ge(1 1 1) interface by the formation of an epitaxial contact. It is expected that SBH at metal/Ge interfaces can be modulated by controlling the interface crystalline structure.

Acknowledgement

This work was partly supported by a Grant-in-Aid for Scientific Research on Priority Areas (No.18063012) from the Ministry of Education, Culture, Sports, Science and Technology in Japan.

References

[1] C.M. Ransom, T.N. Jackson, J.F. DeGelormo, IEEE Electron Dev. 38 (1991) 2695.
[2] A. Dimoulas, P. Tsipas, A. Sotiropoulos, E.K. Evangelou, Appl. Phys. Lett. 89 (2006) 252110.
[3] T. Nishimura, K. Kita, A. Toriumi, Appl. Phys. Lett. 91 (2007) 123123.
[4] T. Nishimura, K. Kita, A. Toriumi, Appl. Phys. Exp. 1 (2008) 051406.
[5] R.R. Lieten, S. Degroote, M. Kujik, G. Borghs, Appl. Phys. Lett. 92 (2008) 022106.
[6] K. Ikeda, Y. Yamashita, N. Sugiyama, N. Taoka, S. Takagi, Appl. Phys. Lett. 88 (2006) 152115.
[7] S. Gaudet, C. Detavernier, C. Lavoie, P. Desjardins, J. Appl. Phys. 100 (2006) 034306.
[8] D.Z. Chi, R.T.P. Lee, S.J. Chua, S.J. Lee, S. Ashok, D.-L. Kwong, J. Appl. Phys. 97 (2005) 113706.
[9] E. Simoen, K. Opsomer, C. Claeys, K. Maex, C. Detavernier, R.L. Van Meirhaeghe, S. Forment, P. Clauws, Appl. Phys. Lett. 88 (2006) 183506.
[10] S. Olive-Mendez, A. Spiesser, L.A. Michez, V. Le Thanh, A. Glachant, J. Derrien, T. Devillers, A. Barski, M. Jamet, Thin Solid Films 517 (2008) 191.
[11] S. M. Sze, Physics of Semiconductor Devices, second ed., Wiley, New York, 1981, p. 245 (Chapter 5).
[12] R.T. Tung, A.F.J. Levi, J.P. Sullivan, F. Schrey, Phys. Rev. Lett. 66 (1991) 72.
[13] R.T. Tung, Mater. Chem. Phys. 32 (1992) 107–133.
[14] I. Ohdomari, K.N. Tu, J. Appl. Phys. 51 (1980) 3735.
[15] J.P. Sullivan, R.T. Tung, M.R. Pinto, W.R. Graham, J. Appl. Phys. 70 (1991) 7403.
[16] R.T. Tung, J.P. Sullivan, E. Schrey, Mater. Sci. Eng. B14 (1992) 266–280.
[17] O. Madelung, Semiconductors: Data Handbook, third ed., Springer, 2004.
[18] E. Simoen, K. Opsomer, C. Claeys, K. Maex, C. Detavernier, R.L. Van Meirhaeghe, P. Clauws, J. Appl. Phys. 104 (2008) 023705.